Contrib Mineral Petrol (2007) 154:119–134
DOI 10.1007/s00410-007-0186-8

ORIGINAL PAPER

Ilmenite composition in the Tellnes Fe–Ti deposit, SW Norway: fractional crystallization, postcumulus evolution and ilmenite–zircon relation

Bernard Charlier · Øyvind Skår · Are Korneliussen · Jean-Clair Duchesne · Jacqueline Vander Auwera

Received: 4 September 2006 / Accepted: 25 January 2007 / Published online: 13 February 2007

Abstract Major and trace element XRF and in situ LA-ICP-MS analyses of ilmenite in the Tellnes ilmenite deposit, Rogaland Anorthosite Province, SW Norway, constrains a two stage fractional crystallization model of a ferrodioritic Fe-Ti-P rich melt. Stage 1 is characterized by ilmenite-plagioclase cumulates, partly stored in the lower part of the ore body (Lower Central Zone, LCZ), and stage 2 by ilmenite-plagioclase-orthopyroxene-olivine cumulates (Upper Central Zone, UCZ). The concentration of V and Cr in ilmenite, corrected for the trapped liquid effect, (1) defines the cotectic proportion of ilmenite to be 17.5 wt% during stage 1, and (2) implies an increase of D_V^{Ilm} during stage 2, most likely related to a shift in fO_2. The proportion of 17.5 wt% is lower than the modal proportion of ilmenite (ca. 50 wt%) in the ore body, implying accumulation of ilmenite and flotation of plagioclase. The fraction of residual liquid left after crystallization of Tellnes cumulates is estimated at 0.6 and the flotation of plagioclase at 26 wt% of the initial melt mass. The increasing content of intercumulus magnetite with stratigraphic height, from 0 to ca. 3 wt%, results from differentiation of the trapped liquid towards magnetite saturation. The MgO content of ilmenite (1.4–4.4 wt%) is much lower than the expected cumulus composition. It shows extensive postcumulus re-equilibration with trapped liquid and ferromagnesian silicates, correlated with distance to the host anorthosite. The Zr content of ilmenite, provided by in situ analyses, is low (<114 ppm) and uncorrelated with stratigraphy or Cr content. The data demonstrate that zircon coronas observed around ilmenite formed by subsolidus exsolution of ZrO_2 from ilmenite. The U-Pb zircon age of 920 ± 3 Ma probably records this exsolution process.

Keywords Ilmenite · Magnetite · Zircon · Laser ablation · Titanium ores · Anorthosite · Rogaland

Introduction

Ilmenite is an early liquidus phase crystallizing after plagioclase in many rocks associated with Proterozoic massif-type anorthosites. It is an excellent monitor of crystallization and fractionation processes because it contains both compatible (Cr and V) and incompatible elements (Mn, Nb, Ta, Zr and Hf). The interpretation of primary ilmenite compositions is, however, complicated by postcumulus re-equilibration (trapped liquid crystallization, exsolution, reaction with magnetite and silicates). From the economic point of view, industrial ilmenite processing is extremely sensitive to the major and trace elements composition, and particularly to the pollutants Cr and Mg.

Communicated by J. Hoefs.

Electronic supplementary material The online version of this article (doi:10.1007/s00410-007-0186-8) contains supplementary material, which is available to authorized users.

B. Charlier (✉) · J.-C. Duchesne · J. Vander Auwera
Department of Geology, B20, University of Liège,
4000 Sart Tilman, Belgium
e-mail: b.charlier@ulg.ac.be

Ø. Skår · A. Korneliussen
Geological Survey of Norway, Leiv Eirikssons vei 39,
7494 Trondheim, Norway

The Rogaland Anorthosite Province (SW Norway) contains numerous Fe-Ti oxide occurrences (Duchesne 1999), but the Tellnes ilmenite deposit is by far the largest and the only one in production today. The mechanism of emplacement of this elongated, trough-shaped ore body has recently been investigated by Charlier et al. (2006). The present study of ilmenite composition from XRF analyses of ilmenite separates and from in situ LA-ICP-MS further refines our understanding of igneous processes in this deposit. It shows the relative contribution of the four main factors, fractional crystallization, liquidus mineralogy, trapped liquid fraction (TLF) and postcumulus re-equilibration, in controlling the ilmenite composition. The amount of MgO in ilmenite and its distribution between ilmenite and melt is examined in detail and compared to the composition of liquidus ilmenite in experiments on ferrobasalts (Snyder et al. 1993; Vander Auwera and Longhi 1994; Toplis and Carroll 1995). The origin of the high amount of ilmenite in the Tellnes deposit is discussed in the light of modelling the variation of ilmenite composition using the Rayleigh equation and calculations of cotectic proportions. The crystallization of small amounts of magnetite and its influence on ilmenite composition is also examined. Finally, new light is shed on the age of the Tellnes ilmenite deposit, which hitherto has been believed to be 10 Ma younger than other plutons of the Rogaland Anorthosite Province (Schärer et al. 1996).

Geological background

The Tellnes ilmenite deposit belongs to the Rogaland Anorthosite Province, exposed in the Sveconorwegian orogen in southwest Norway (Fig. 1). Anorthosite-kindred plutonic rocks intruded granulite-facies gneisses at around 930 Ma (Schärer et al. 1996) in post-collisional regime (Duchesne et al. 1999; Bingen et al. 2006). They postdate final Sveconorwegian convergence and regional metamorphism by some 40 Ma (Bingen and van Breemen 1998; Bingen and Stein 2003), and have not been overprinted during the Caledonian orogeny. Fabrics and deformation observed in the Rogaland Anorthosite Province are related to the diapiric emplacement of plutons (Duchesne et al. 1985; Barnichon et al. 1999) and to gravity-induced subsidence of denser rocks bodies (e.g. Bolle et al. 2002).

The Tellnes deposit is located in the central part of the Åna-Sira anorthosite (Krause et al. 1985). Tellnes is a world-class titanium mineral deposit: it has a yearly production of 800,000 tons of ilmenite concentrate, equivalent to 7% of the total production of titanium minerals in the world by TiO_2 content. The ilmenite is primarily used for the production of titanium pigment by the sulphate process. The intrusion outcrops as a $2{,}700 \times 400$ m sickle-shaped body with a synclinal cross-section (Fig. 2). This morphology is interpreted as resulting from the gravity-induced subsidence of a subhorizontal sill (Charlier et al. 2006). The parental magma had the composition of a Fe-Ti-P-rich ferrodiorite (jotunite), as indicated by the presence of fine-grained rocks at the margins of the intrusion and the pressure of emplacement, constrained by phase relations, is around 5 kbar (Charlier et al. 2006). The Tellnes deposit yields a zircon U-Pb age of 920 ± 3 Ma, some 10 Ma younger than the average zircon age of 931 ± 2 Ma for three of the large hosting anorthosite plutons (Schärer et al. 1996). It is cross-cut by two doleritic dykes (616 ± 3 Ma) that are related to the opening of the Iapetus Ocean (Bingen et al. 1998).

Sampling and petrography

Samples were selected along 16 drill cores in three SSW–NNE cross-sections perpendicular to the elongation of the ore body, labeled 800, 1200 and 1600 (Fig. 2). Petrographic studies were carried out on polished thin sections for all rocks.

The Tellnes ore is a massive, medium-grained (0.5–2 mm) ilmenite-rich noritic cumulate. The norite is homogeneous at the outcrop scale and rarely displays conspicuous modal layering. A detailed petrographic study presented by Charlier et al. (2006) concluded that plagioclase and ilmenite were the first liquidus minerals, followed by both orthopyroxene and olivine. Based on this succession of cumulus minerals, the ore body has been subdivided into a Lower Central Zone (LCZ) where plagioclase and ilmenite are cumulus phases (pi-C following the terminology of Irvine 1982) and an Upper Central Zone (UCZ), where plagioclase, ilmenite, orthopyroxene and olivine are cumulus phases (piho-C) (Fig. 2).

The primary texture of ilmenite has been severely modified by subsolidus grain boundary migration and textural equilibration during deformation and recrystallization of the intrusion. Ilmenite is usually interstitial to the main silicate minerals. As a result of recrystallization, distinction between cumulus and intercumulus ilmenite grains is not possible. The proportion of ilmenite (eFig. 1) is high in the central part of the body (40–50 wt%) and decreases continuously towards the margins (to as low as ca. 15 wt%). Mining data of the Cr concentration in ilmenite (Fig. 3a–c), which decreases continuously from the lower to the upper part of the

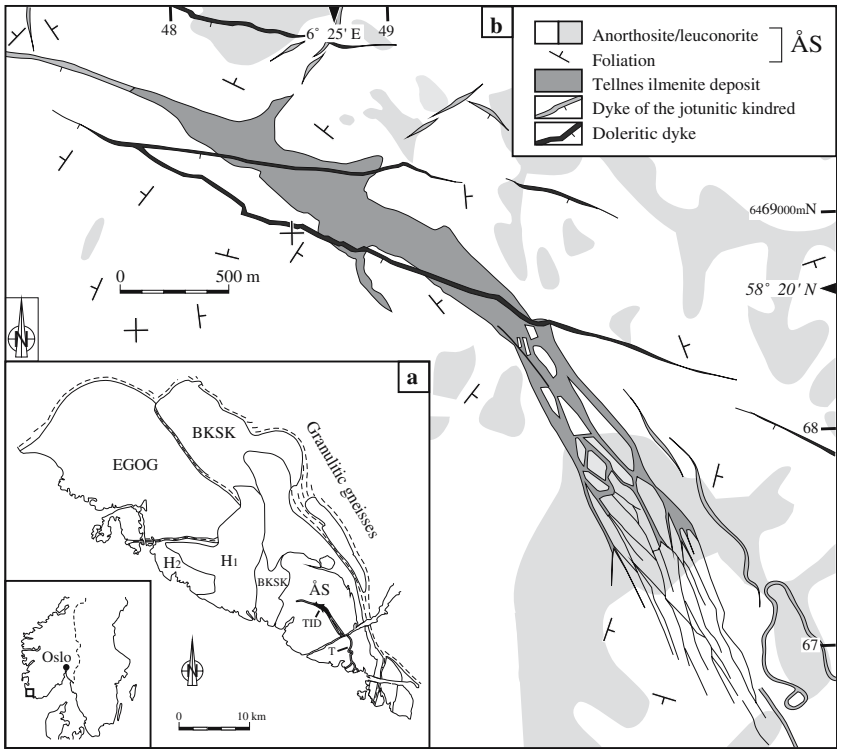

Fig. 1 **a** Geological map of the Rogaland Anorthosite Province (after Bolle 1996) showing the location of the Tellnes ilmenite deposit in the central part of the Åna-Sira anorthosite (ÅS). $H_1 + H_2$ Håland-Helleren anorthosites, *EGOG* Egersund-Ogna anorthosite, *BKSK* Bjerkreim-Sokndal layered intrusion, *T* Tellnes "main dyke"; *TID* Tellnes ilmenite deposit. **b** Geological map of the Tellnes ilmenite deposit (after Krause et al. 1985). Grid is the EUREF89 kilometric UTM

intrusion, displays spatial variations concordant with the limit between LCZ and UCZ (Fig. 2).

Intercumulus minerals (clinopyroxene, magnetite, biotite, apatite and amphibole) are commonly more abundant at the margins of the ore body where the TLF is higher. This is particularly obvious for apatite, as expressed by the P_2O_5 content of bulk cumulates (Charlier et al. 2006). Even if the proportion of magnetite is commonly higher at the margins, mining data of the magnetite content in Tellnes cumulates show that the main feature is an increase in its modal abundance towards the top of the intrusion (Fig. 3d–f). Two types of magnetite are distinguished: small grains associated with sulphides and large grains (ca. 0.5 mm) containing exsolution lamellae of pleonaste (aluminous spinel) which appear simultaneously with olivine and large prismatic orthopyroxene in the UCZ. The magnetite content is close to 0–0.3% in LCZ (essentially small grains) and reaches values slightly higher than 3% in the UCZ (essentially large grains).

Ilmenite and magnetite display various subsolidus re-equilibration textures (Fig. 4). Ilmenite contains lenses of exsolved hematite and could thus be referred to as hemo-ilmenite. Pleonaste is common as exsolved lenses in ilmenite (Fig. 4a) or as larger grains inside or outside ilmenite grains, interpreted as representing external granule exsolution. Ilmenite may also be rimmed by a thin zircon corona, 1–5 μm wide but locally up to 20 μm in samples close to the margin with the host anorthosite (Fig. 4a–c). Baddeleyite is also common as small euhedral grains included in ilmenite. A decrease in the hematite lamellae in ilmenite close to the exsolved pleonaste (Fig. 4a) and to the sulphides (Fig. 4d) as well as to magnetite are observed (Fig. 4f). Re-equilibration between ilmenite and olivine or orthopyroxene is not apparent from microtextures, but strong re-equilibration is seen between ilmenite and magnetite. The hematite content (Fe_2O_3) of ilmenite decreases towards the margin with magnetite. Ilmenite close to the contact with magnetite is dotted with pleonaste microcrystals. The core of some of these pleonastes is locally constituted by magnetite (Fig. 4e, f). This texture is commonly interpreted to result from the reaction of ulvöspinel (Fe_2TiO_4) in magnetite with hematite in ilmenite to form a rim of a spinelliferous ilmenite exsolved from the magnetite (Duchesne 1972). This reaction reduces both the Ti content of magnetite and the hematite content of ilmenite. Because of the small proportion of magnetite relative to ilmenite, this reaction has mainly changed the primary composition of magnetite into a Ti-poor variety, without significantly affecting the composition of the ilmenite (Frost et al. 1988).

Analytical procedures

Twenty-one samples have been selected from cross-sections 1200 and 1600 for mineral separation (Fig. 2).

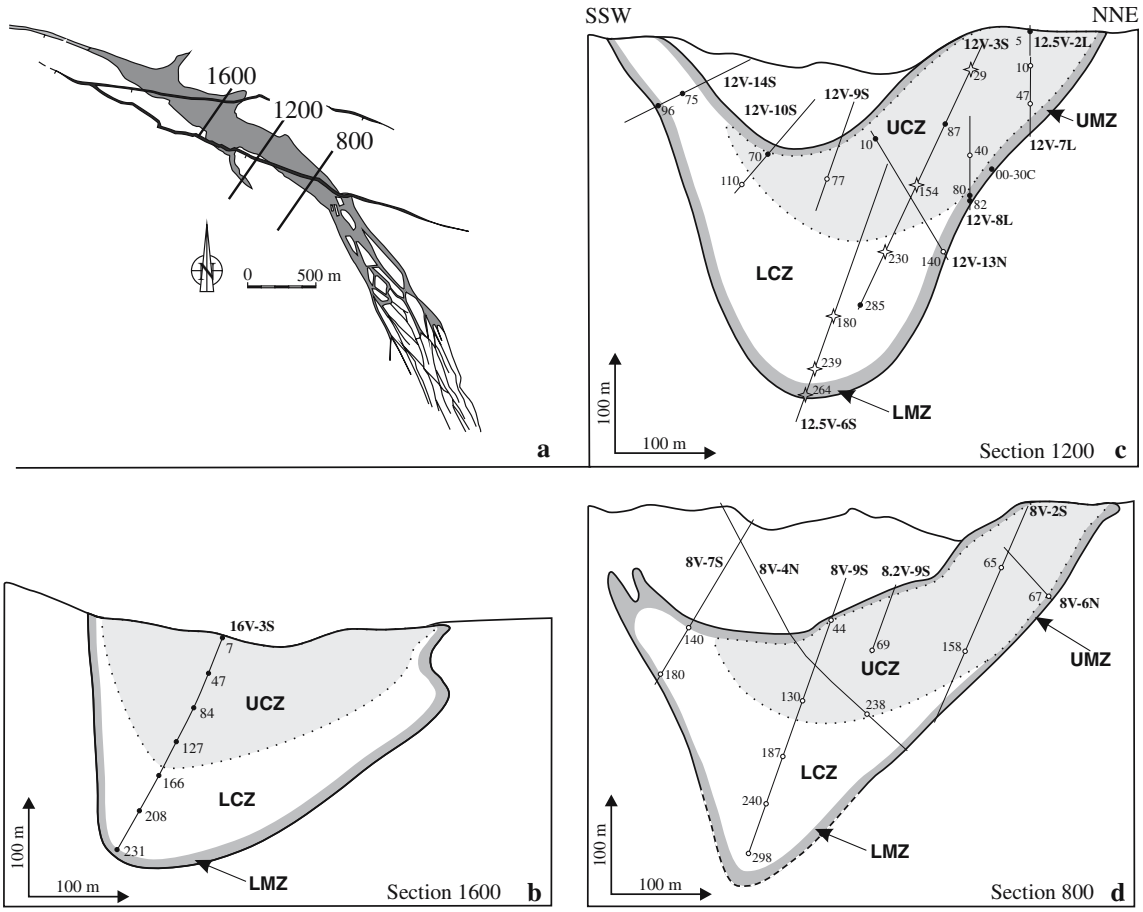

Fig. 2 **a** Location of the three selected cross sections on the geological map of the Tellnes ilmenite deposit (same legend as Fig. 1b); **b–d** Spatial distribution of selected drill holes and samples (numbers give their depth) for ilmenite analyses in cross sections 1600, 1200 and 800 (*open circles* are XRF analyses on mineral separates, *filled circles* are LA-ICP-MS in situ analyses and *stars* have been analysed by both methods). The dashed base of section 800 has not been intersected by drilling and is inferred. *LCZ* lower central zone, *UCZ* upper central zone, *UMZ* upper marginal zone, *LMZ* lower marginal zone

Separation of ilmenite (60–150 μm) was performed using heavy liquids (bromoform and Clerici's solution) and a Frantz isodynamic magnetic separator. Final purification was achieved by handpicking under the microscope. Samples ground in an agate mortar were analysed for major elements (Si, Ti, Al, Fe, Mn, Mg) by XRF on lithium-borate fused glass and for trace elements (V, Cr, Zr, Nb) on pressed powder pellets (eTable 1). International Fe-Ti oxide reference materials (SARM 59 and 12, IGS 31 and 32, GBW 07226), samples 16716 G/91, V4–1, 16717 provided by TITANIA A/S, as well as synthetic standards and in-house standards were used for calibration.

Ilmenite from 29 samples in sections 800 and 1200 was also analysed in polished rock slabs by LA-ICP-MS at the Geological Survey of Norway (eTable 2) using a Finnigan ELEMENT 1 single collector high-resolution instrument alimented by a Finnigan 266 nm UV-laser. The laser was operated at a frequency of 10 Hz and an energy of about 1.0 mJ. A beam of 20 μm in diameter was rastered over an area of about 100 × 200 μm at the surface of selected ilmenite grains. This method provides an analysis of the bulk composition of ilmenite including hematite exsolution lamellae. Helium gas (0.4 l min^{-1}) was used to flush the sample chamber, and mixed with Ar gas (0.9 l min^{-1}) for introduction of the aerosol in the ICP-MS. Each composition reported is an average of three to six analyses. Ilmenite grains in a single sample display very homogeneous compositions.

Zr, Hf and Ta were measured in the nominal mass resolution settings of 300 M/ΔM (Low Resolution), whereas all the other elements where measured in 3,000 M/ΔM (Medium Resolution) to avoid interference problems. The measurement time of each analysis was 30 s for gas blank acquisition and 60 s data acquisition for the sample. For Mn, Mg, V, Cr, Zr, Hf and Nb, the synthetic titanite glass standard (TIT–200)

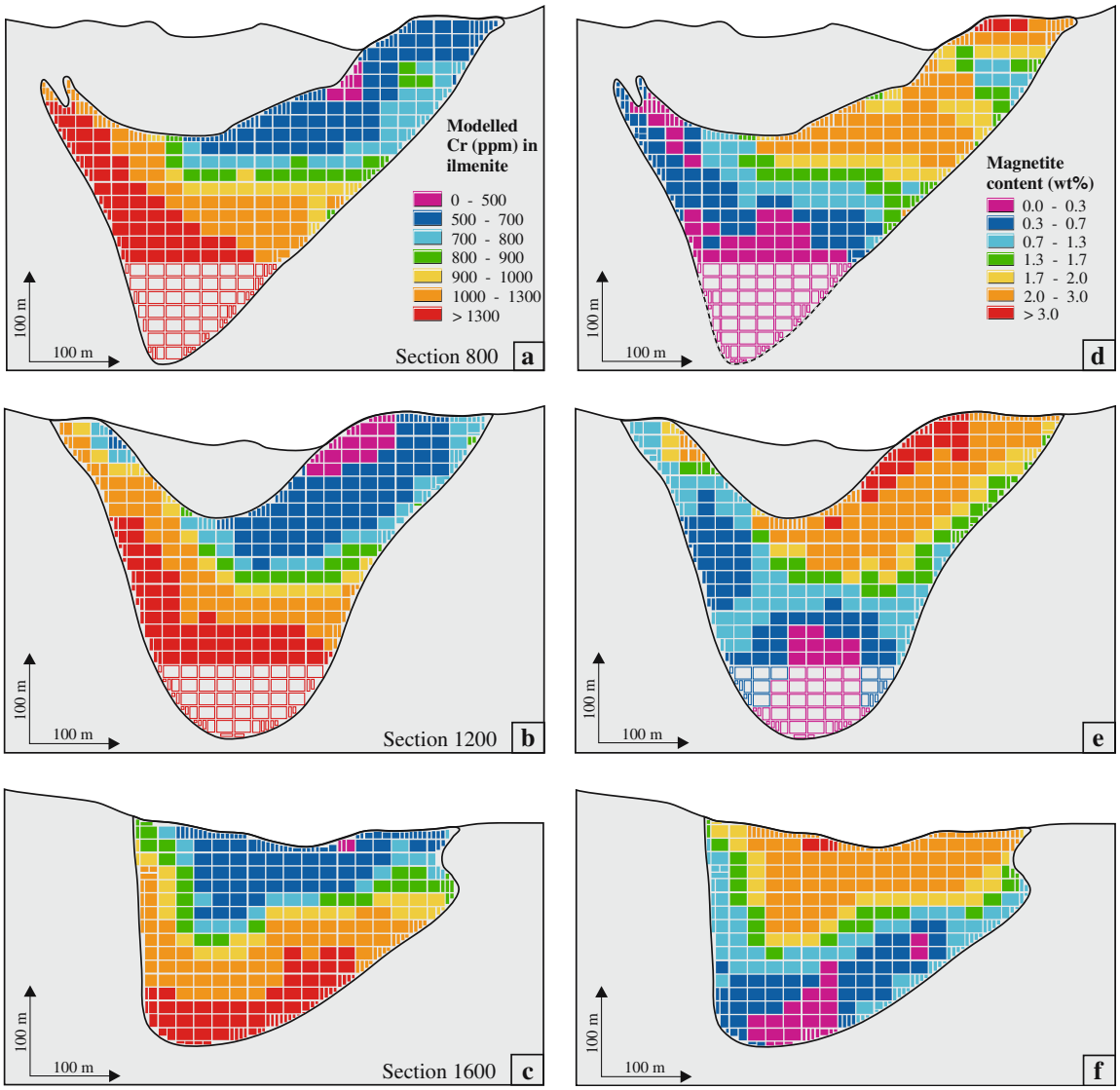

Fig. 3 **a–c** Cr content in ilmenite in sections 800, 1200 and 1600 of the Tellnes ilmenite deposit; **d–f** Spatial distribution of the magnetite content (wt%) in sections 800, 1200 and 1600 of the Tellnes ilmenite deposit. The local anomalously low proportion of magnetite in the upper part of section 800 results from the presence of large xenoliths of the host anorthosite. *Filled 3-D rectangular blocks* are modelled by interpolation of about 5,000 analyses of Cr in ilmenite concentrate and of the magnetite content after magnetic separation (unpublished database of TITANIA A/S; DATAMINE® software); *open blocks* have not been intersected by drill cores and are inferred

(Ødegaard et al. 2005) was used as external standard, and Ti as internal standard. For the elements Al, Si and Ta, the NIST 612 was used as external standard and Nb as internal standard. Mg was not determined in six samples due to analytical problems. For data reduction, the GLITTER (http://www.glitter-gemoc.com/) software package (Van Achterberg et al. 2001) was used. The calibration standards were analysed at the beginning and at the end of each sequence. To control the accuracy and precision of the analysis, the international standard BHVO-2 was analysed together with the unknown samples. From the repeated analysis of the BHVO-2 standard, the accuracy of the trace elements V, Cr, Zr and Nb are in the range 1–7%. The accuracy is 16% for Hf and 20% for Ta. The relative standard deviation for all trace elements are <10% except for Zr (17%).

Six samples have been analysed by both analytical methods. Results obtained by XRF and LA-ICP-MS are extremely similar, except for Mn, which is 20% higher with LA-ICP-MS and for Zr, which does not correlate (see interpretation below).

Orthopyroxene separates (eTable 3) from LCZ and marginal zones were analysed for major elements by

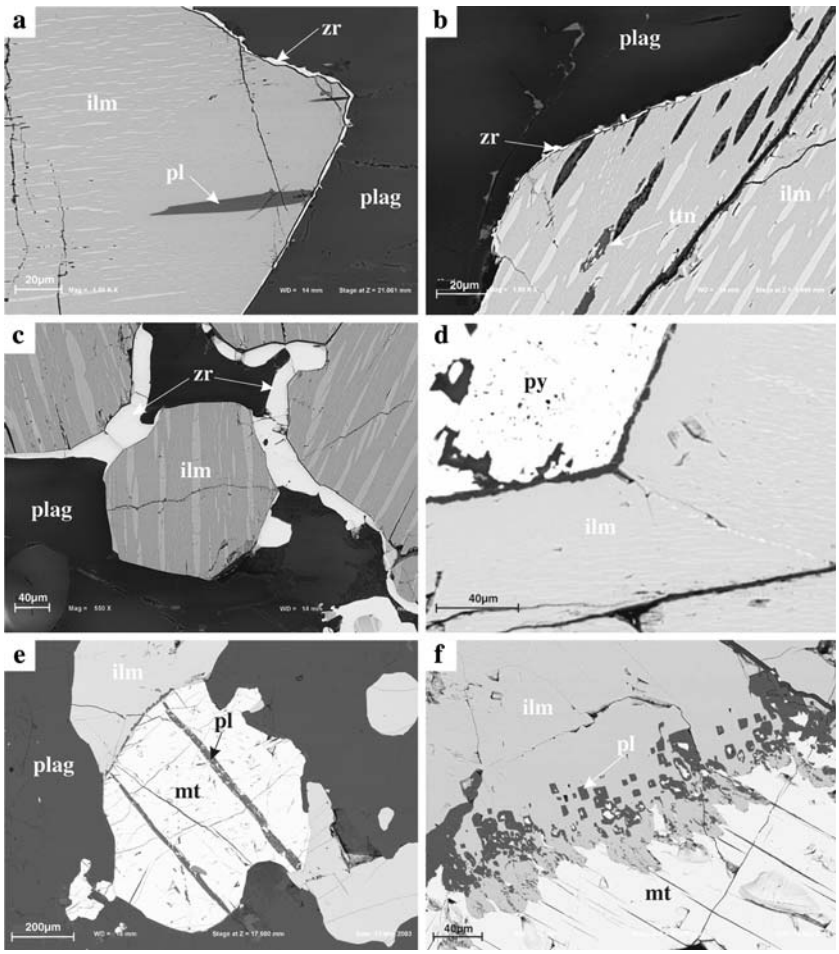

Fig. 4 Backscattered electron (BSE) images of polished thin sections showing main textures of Fe-Ti oxides in the Tellnes ilmenite deposit. Phases were identified with energy dispersive X-ray spectrometry. **a** Ilmenite grain in contact with plagioclase, with a large pleonaste exsolution wedge and a zircon corona. Note the decrease in the amount of hematite towards the pleonaste (sample 12 V–13 N, 140); **b** Ilmenite with exsolved hematite locally altered to titanite. A later thin rim of zircon is developed between ilmenite and plagioclase (sample 99–23b); **c** Ilmenite with two generations of exsolved hematite and thick zircon coronas (sample 99–23b); **d** Ilmenite in contact with pyrite. The *black line* between the two minerals is a polishing artifact. Note the decrease of hematite exsolutions towards pyrite (sample 8 V–9 S, 130); **e** Magnetite grain with thick lamellae of pleonaste (sample 8 V-4 N, 238); **f** Detail of the contact between ilmenite and magnetite with a pleonaste rim. Note relicts of the magnetite inside some of the pleonaste cubes and the irregular margin of magnetite (sample 8 V-4 N, 238). Mineral abbreviations: *ilm* ilmenite, *mt* magnetite, *plag* plagioclase, *py* pyrite, *pl* pleonaste, *ttn* titanite, *zr* zircon

XRF on lithium-borate fused glass on pressed powder pellets. Orthopyroxene from UCZ was analysed by microprobe analyses performed on a Cameca SX50 at the University of Bochum (Germany) because of mineral separation contaminated by olivine. An accelerating voltage of 15 kV, a beam current of 15 nA and a focused beam were used.

Results

Ilmenite composition

Data for major and trace element in ilmenite are reported in eTables 1, 2. Ilmenite in sample 12.5 V-6 S (264), situated at the contact with the host anorthosite (Fig. 2c), has a different composition compared to other samples with, for example, lower MgO and Cr contents (0.54 wt% and 93 ppm, respectively) and higher MnO (0.44 wt%). This is consistent with the interpretation of this sample as representing the chilled parental magma of the deposit (Charlier et al. 2006). This composition is believed to result from equilibrium crystallization of a melt.

The MgO content of ilmenite varies between 1.42 and 4.44 wt% (eFig. 2a–c). From the lower to the upper part, MgO first increases when plagioclase and ilmenite are cumulus minerals (LCZ) and then decreases when orthopyroxene and olivine appear as cumulus phases (UCZ). Samples from the marginal

zones have systematically lower MgO contents. The hematite content varies slightly between Hem_{10} and Hem_{14} and is systematically higher in samples from the margins of the ore body.

Cr ranges from 2,065 to 283 ppm (eFig. 2a–c) and, as also shown by Fig. 3a–c, decreases continuously from the lower to the upper part of the intrusion. V (1,192–1,555 ppm) displays similar trends (not shown). Their compatible behaviour results from the high partition coefficients of these elements in ilmenite. Even if MnO, Nb, Ta, Zr and Hf are present in significant amounts in ilmenite, these elements behave globally as incompatible components. The concentrations of these elements increase up to the top of the intrusion and they are enriched at the margin of the ore body. The ranges of composition are 0.24–0.33 wt% for MnO, 47–111 ppm for Nb (eFig. 2a–c) and 4.1–7.0 ppm for Ta. Zr appears to have an unsystematic behaviour. Indeed, data from XRF and LA-ICP-MS analyses are completely uncorrelated. This inconsistency is further documented below. The LA-ICP-MS Hf analyses correlate with the LA-ICP-MS Zr analyses and ranges from 1.1 to 8.5 ppm. Sc displays a very restricted range of concentration from 27 to 49 ppm and its variation is closer to the other incompatible elements.

Orthopyroxene composition

The Mg# of orthopyroxene (eFig. 3) is rather homogeneous in the central parts of the ore body (Mg# = 75–76) and is significantly lower in marginal zones, down to Mg# = 65. No systematic evolution with stratigraphic height may be clearly evidenced.

Discussion

The composition of cumulus ilmenite

Variations of ilmenite compositions are primarily considered to result from fractional crystallization. However, in cumulates from the Tellnes ilmenite deposit, the TLF is the main controlling factor on plagioclase and bulk cumulate compositions (Charlier et al. 2006). The TLF varies between 20 and 80% and is higher at the margins of the ore body. It reaches 100% in the chilled sample 12.5 V-6 S (264). This trapped liquid is responsible for the lower ilmenite content at the margins with the anorthosite due to the dilution effect of an increasing proportion of trapped liquid poorer in TiO_2 than the cumulus assemblage. Consequently, the composition of the cumulus ilmenite must also be influenced by the trapped liquid. The ilmenite composition obtained from the mineralogical separates is representative of the composition of cumulus ilmenite plus a variable proportion of ilmenite crystallized from trapped liquid, either as overgrowths or as new discrete grains. LA-ICP-MS data are also considered to represent the composition of re-equilibrated ilmenite because they are homogeneous in a single sample. Any possible original primary zoning and/or overgrowth on cumulus ilmenite have been completely obliterated by diffusion and recrystallization.

Knowledge of the primary composition of cumulus ilmenite is crucial for the reconstruction of fractionation processes. This composition of the cumulus ilmenite ($C_{\text{cum ilm}}$) can be calculated by mass balance. The concentration C of any element in analysed ilmenite ($C_{\text{bulk ilm}}$) is

$$C_{\text{bulk ilm}} = C_{\text{cum ilm}} X_{\text{cum ilm}} + C_{\text{interst ilm}} X_{\text{interst ilm}}$$

and its concentration in cumulus ilmenite is

$$C_{\text{cum ilm}} = [C_{\text{bulk ilm}} - C_{\text{interst ilm}} \cdot X_{\text{interst ilm}}]/X_{\text{cum ilm}}$$

with $C_{\text{interst ilm}}$ the concentration of any element in ilmenite crystallized from the trapped liquid, $X_{\text{cum ilm}}$ and $X_{\text{interst ilm}}$ the fraction of cumulus and interstitial ilmenite, respectively, of the bulk ilmenite content in the cumulate, with

$$X_{\text{interst ilm}} = 1 - X_{\text{cum ilm}}.$$

This fraction of cumulus ilmenite is

$$X_{\text{cum ilm}} = \text{TiO}_{2\ \text{cum}}/\text{TiO}_{2\ \text{bulk}}$$

with $TiO_{2\ cum}$ being the TiO_2 contribution of the cumulus assemblage to the TiO_2 content of the bulk cumulate ($TiO_{2\ bulk}$, eTables 1, 2), which may be expressed as

$$\text{TiO}_{2\ \text{cum}} = \text{TiO}_{2\ \text{bulk}} - \text{TiO}_{2\ \text{interst}}$$

with $TiO_{2\ interst}$ being the TiO_2 contribution of the trapped liquid to the TiO_2 content of the bulk cumulate ($TiO_{2\ bulk}$). If we know the TLF and its TiO_2 content ($TiO_{2\ TL}$), we can obtain $TiO_{2\ interst}$

$$\text{TiO}_{2\ \text{interst}} = \text{TiO}_{2\ \text{TL}}\text{TLF}.$$

The TLF in each cumulate can be calculated from the P_2O_5 content of bulk cumulates ($P_2O_{5\ bulk}$; eTables 1, 2) since P_2O_5 in the trapped liquid ($P_2O_{5\ interst}$) is exclusively present in intercumulus apatite

$TLF = P_2O_{5\ bulk}/P_2O_{5\ interst}$.

For small degree of fractionation, $P_2O_{5\ interst}$, $TiO_{2\ interst}$ and $C_{interst\ ilm}$ can be considered as the composition of the parental magma and its ilmenite, respectively (sample 12.5 V-6 S, 264; eTable 1). Consequently, for the most primitive ilmenite (sample 12.5 V-6 S, 239; eTable 1) in which $Cr_{bulk\ ilm}$ = 2,065 ppm, TLF = 54%, $TiO_{2\ TL}$ = 5.39 wt%, $TiO_{2\ bulk}$ = 16.73 wt%, we obtain $Cr_{cum\ ilm}$ = 2,477 ppm. The trapped liquid shift thus induces a 20% decrease of the Cr content in ilmenite. Except for samples from marginal zones which may contain 80% trapped liquid (Charlier et al. 2006) and which will not be considered in the modelling of fractionation processes, this 20% trapped liquid shift is the maximum correction for any element because sample 12.5 V-6 S (239) has the highest TLF among samples from central zones (LCZ and UCZ), it has the most primitive ilmenite composition and thus the largest difference with the trapped liquid composition. Finally, Cr is the most compatible element and thus the difference between $C_{cum\ ilm}$ and $C_{interst\ ilm}$ is maximum for this element.

The assumptions that $P_2O_{5\ interst}$, $TiO_{2\ interst}$ and $C_{interst\ ilm}$ can be considered to be the composition of the parental magma and its ilmenite respectively are valid for the most primitive cumulates and become increasingly wrong for more evolved cumulates because: (1) the P_2O_5 content of the residual melt continuously increases with fractionation because apatite is not a liquidus phase, (2) the TiO_2 content decreases due to ilmenite fractionation; (3) the concentration of any element in interstitial ilmenite varies because of the variation of the trapped liquid composition and (4) new intercumulus phases may appear (e.g. magnetite in the UCZ). Consequently, the correction for the trapped liquid shift is accurate for the most primitive cumulates and is more and more overestimated with differentiation.

Data for the three different sections are illustrated in Fig. 5 for the Cr content of ilmenite as a function of depth. Values corrected for the trapped liquid shift are increasingly higher than uncorrected values with depth. Even if the correction is overestimated in UCZ, the difference between the two values becomes negligible. Note that section 1200 has the most primitive ilmenite composition (Cr = 2,480 ppm). This is probably because the first crystallizing liquidus phases accumulated here, in what could originally have been the deepest part of the Tellnes magma chamber.

Stratigraphic variation of cumulus ilmenite composition: a Rayleigh fractionation model

The continuous decrease in compatible element concentrations with stratigraphic height (e.g. Cr, Fig. 5) is a clear indication that fractional crystallization was the main mechanism of differentiation. Differentiation by Rayleigh fractionation is evidenced in the log Cr-log V in ilmenite diagram of Fig. 6 where samples belonging to the same fractionation interval plot on linear trends. Ilmenite data, corrected for the trapped liquid shift, display two different linear trends for the two cumulus assemblages pi-C and piho-C. This implies that bulk partition coefficients for the two fractionating cumulus assemblages are significantly different.

Modelling of ilmenite composition may thus be performed using the Rayleigh (1896) equation:

$$C_i^{Liq} = C_i^0 F^{(D-1)}$$

and thus,

$$C_i^j = D_i^j C_i^0 F^{(D-1)}$$

where C_i^{Liq} and C_i^j are the instantaneous concentrations of element i in the melt and in mineral j respectively, C_i^0 is the initial concentration of i in the parental

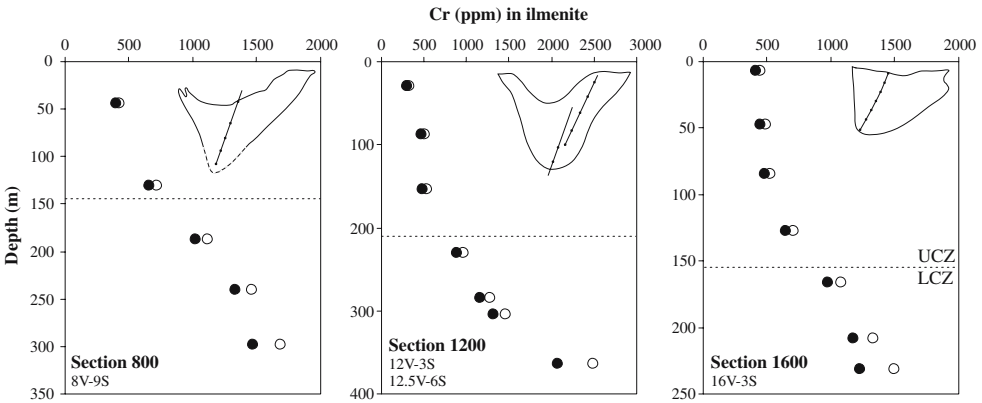

Fig. 5 Cr content in ilmenite (ppm) as a function of depth in the drill core (in meters) in sections 800, 1200 and 1600 of the Tellnes deposit. *Open circles* are values corrected for the trapped liquid shift; *filled circles* are uncorrected values

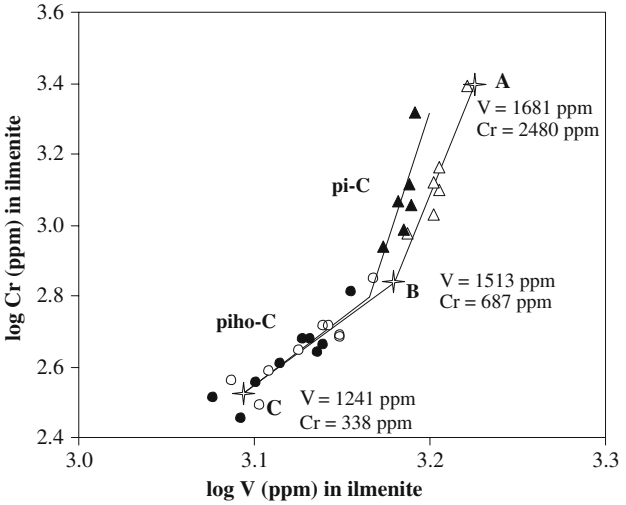

Fig. 6 log Cr versus log V in ilmenite of the Tellnes deposit with linear regressions for pi-C and piho-C corrected for the trapped liquid shift *(open symbols)* and uncorrected (*filled symbols*). Note similar linear regression for piho-C corrected and uncorrected from the trapped liquid shift. *A* is the most primitive corrected ilmenite composition; *B* is the intersection between the two linear trends of corrected compositions and *C* is the average of the two most evolved corrected ilmenite compositions

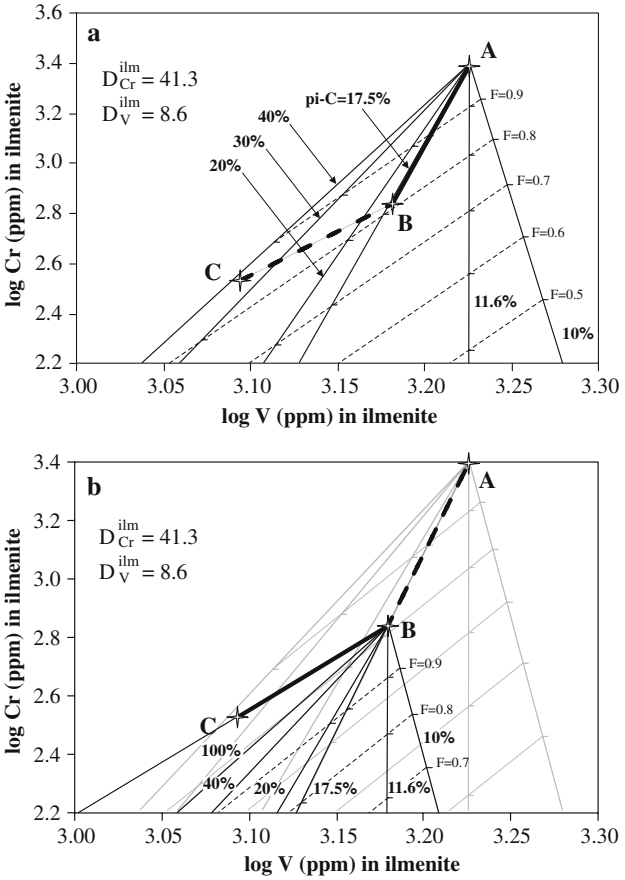

Fig. 7 Model for the Cr and V concentrations in ilmenite of the Tellnes deposit for various cotectic proportions of ilmenite. **a** Model 1 from *A* to *B* for ilmenite in pi-C. **b** Model 2 from *B* to *C* for ilmenite in piho-C. *A*–*B*–*C* and heavy linear regressions are from Fig. 9. *F* is the fraction of residual liquid

magma, *F* is the fraction of residual liquid and *D*, the bulk partition coefficient between the cotectic cumulate and the melt, i.e. $D = \Sigma X^j \cdot D_i^j$, with X^j the mass fraction of mineral *j* in the cumulate and D_i^j the partition coefficient of element *i* between mineral *j* and melt.

The composition of the parental magma of the deposit is constrained by the chilled margin composition, and the partition coefficients between ilmenite and liquid can be calculated from the composition of the most primitive cumulus ilmenite corrected for the trapped liquid shift. Therefore, application of the Rayleigh equation permits quantitative assessment of the fraction of residual liquid (*F*) left after crystallization of the exposed portion of the deposit. Finally, because the bulk partition coefficients of cumulates are related to cotectic proportions of liquidus phases, the Rayleigh equation can be used to constrain these proportions.

A two-step model must be applied (Fig. 7a, b) to match the two linear trends in Fig. 6. The first path (Fig. 7a) characterizes the fractionation of pi-C from the parental magma composition, and starts from the most primitive ilmenite. The second path (Fig. 7b) represents the crystallization of piho-C, starting from the intersection between the two linear regressions (Fig. 6) where ilmenite contains 687 ppm Cr and 1,513 ppm V. Because plagioclase is the only other liquidus phase in LCZ, Cr and V can be considered to be exclusively present in ilmenite. Partition coefficients for Cr and V in ilmenite are calculated by dividing the composition of the most primitive ilmenite by the composition of the parental magma. Several curves for the variation of log Cr versus log V in ilmenite are reported for various cotectic proportions of ilmenite (Fig. 7a). It emerges from this figure that the compositional variation of ilmenite best fits a cotectic proportion of ilmenite of 17.5% during the crystallization of pi-C (when bulk partition coefficients are 7.2 and 1.5 for Cr and V, respectively). Note that the model is very sensitive to small variations in the ilmenite proportions and that, for example, 11.6% ($D_V^{Bulk} = 1$) or 20% of ilmenite result in very different paths.

This cotectic proportion of ilmenite (17.5%) is significantly lower than the calculated proportion of cumulus ilmenite (proportion of ilmenite in the cumulate corrected for the diluting effect of trapped liquid) in the ore body which is around 50 wt% (Charlier et al. 2006). This strongly implies that

ilmenite is not present in cotectic proportions in the ore body but has been concentrated at the bottom of the chamber. The fraction of residual liquid F left after the crystallization of pi-C is ca. 0.8 (Fig. 7a).

For the second fractionation path of piho-C (Fig. 7b), considering that bulk partition coefficients for V and Cr are similar to that in pi-C, the linear trend fits a cotectic proportion of ilmenite higher than 100%, which is obviously incorrect. Bulk partition coefficients for V and/or Cr in piho-C are thus higher to that in pi-C. Two factors may be responsible for this variation: (1) the appearance of a new crystallizing phase with high partition coefficients for Cr and V or (2) an increase of D_{Cr}^{Ilm} and/or D_{V}^{Ilm}. Based on petrographic observations, both olivine and orthopyroxene appear as new cumulus phases after pi-C (Charlier et al. 2006). However, even if their partition coefficients for Cr and V are higher than that for plagioclase (e.g. $D_{Cr}^{Opx} = 5$ at around 5 kbar in Vander Auwera et al. 2000; $D_{V}^{Opx} < 1$, e.g. Kennedy et al. 1993), they remain too low to significantly affect D_{Cr}^{Bulk} and D_{V}^{Bulk}. Magnetite is another possible candidate. As previously shown (Fig. 3), small amounts of intercumulus magnetite crystallize together with cumulus orthopyroxene and olivine. However, magnetite is a cumulus phase in troctolitic cumulates belonging to MCU IVa in the nearby Bjerkreim–Sokndal layered intrusion (Fig. 1; Wilson et al. 1996) where D_{Cr}^{Mt} was estimated to be between 520 and 710 (Jensen et al. 1993). Consequently, if 3% magnetite with $D_{Cr}^{Mt} = 600$ is added to the cumulus assemblage in piho-C, D_{Cr}^{Bulk} is increased by 18 and will thus be ca. 25. The amount of fractionation required to produce the variation of the Cr content in ilmenite from B (687 ppm) to C (338 ppm) in piho-C (Fig. 6) comes out at $F = 0.97$. This is inconsistent with the volume of piho-C (Fig. 2), which is similar to that of pi-C after which $F = 0.8$. The intercumulus status of magnetite is thus confirmed on geochemical grounds. Its increasing content with stratigraphic height (Fig. 3) results from the evolution of the trapped liquid composition which becomes closer to magnetite saturation.

The reason for variation of D_{Cr}^{Bulk} and/or D_{V}^{Bulk} in the second fractionation path might be a different cotectic proportion of ilmenite in piho-C but more certainly variation of fO_2 with differentiation. Indeed, data from Toplis and Corgne (2002) in ferrobasalts have shown that D_{V}^{Mt} increases by approximately one order of magnitude with decreasing oxygen fugacity from NNO + 2.6 to NNO-0.7. It is thus reasonable to consider that fO_2 also affects D_{V}^{Ilm}. Considering a cotectic proportion of ilmenite in piho-C similar to that in pi-C (17.5%), the same D_{Cr}^{Ilm}, the trend for piho-C is reproduced for $D_{V}^{Ilm} = 14$.

Until more data are available for variation of partition coefficients in ilmenite with oxygen fugacity and since the volume of pi-C (LCZ) is similar to that of piho-C (UCZ) (Fig. 2), the fraction of residual liquid after the crystallization of Tellnes cumulates is estimated at ca. 0.6 of the initial melt.

MgO in ilmenite and postcumulus re-equilibration

Partition coefficient for MgO between ilmenite and melt

The MgO partitioning between ilmenite and coexisting melt (D_{MgO}^{Ilm}) has been determined using experimental data in which ilmenite was a liquidus phase. Data from Snyder et al. (1993), Vander Auwera and Longhi (1994) and Toplis and Carroll (1995) are exploited here because they all deal with ferrobasaltic (or jotunitic) liquids, which are compositionally very close to the Tellnes parental magma. Pressure has negligible influence on D_{MgO}^{Ilm} (Vander Auwera et al. 2003). Moreover, experiments by Toplis and Carroll (1995) performed at fO_2 between FMQ + 1 and FMQ-2 do not show any systematic variation of D_{MgO}^{Ilm} with fO_2. The MgO content of the liquid is thus probably the main controlling variable on ilmenite composition. Figure 8 displays the MgO content of ilmenite obtained experimentally as a function of the MgO content of the liquid in equilibrium with ilmenite. D_{MgO}^{Ilm} is quite consistent in the three datasets: 1.35 (Snyder et al. 1993), 1.39 (Vander Auwera and Longhi 1994) and 1.32 (Toplis and Carroll 1995). Cawthorn and Biggar (1993) obtained $D_{MgO}^{Ilm} = 1.5$ from experiments on TiO_2-rich basalts, a value in good agreement with the three datasets. Experimental data of Toplis et al. (1994) on the role of phosphorous in crystallization processes of basalt tends to show a decrease of D_{MgO}^{Ilm} with increasing P_2O_5 content of the melt. However, D_{MgO}^{Ilm} remains > 1 and the Tellnes melt does not reach P_2O_5 content higher than 0.7/0.6 = 1.17 wt% P_2O_5 ($C_i^{Liq} = C_i^0/F$ for incompatible elements). Melts in the study of Vander Auwera and Longhi (1994) in which $D_{MgO}^{Ilm} = 1.39$ have 0.65–2.32 wt% P_2O_5. In any case, at the time of crystallization, ilmenite will have a higher MgO content than the liquid with which it is in equilibrium.

MgO in ilmenite in the Tellnes deposit

The stratigraphic variation of the MgO content in ilmenite from the Tellnes ilmenite deposit seems to be controlled by fractional crystallization. Figure 9 shows the MgO in ilmenite plotted as a function of Mg# in orthopyroxene (eTable 3). Both values increase up-

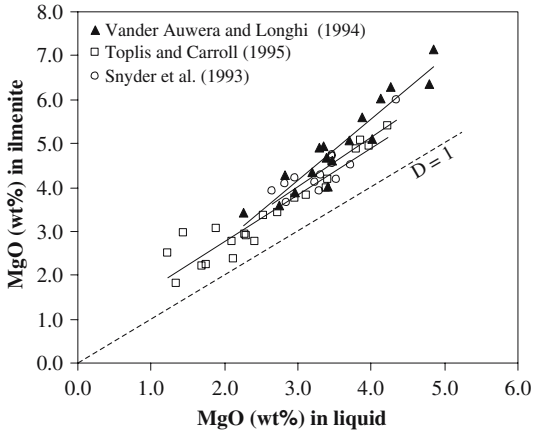

Fig. 8 MgO (wt%) in ilmenite as a function of MgO (wt%) in melt in equilibrium with ilmenite in the experiments on ferrodioritic (jotunitic) magma of Snyder et al. (1993) (number of samples $n = 13$; linear regression $r^2 = 0.74$), Vander Auwera and Longhi (1994) ($n = 17$; $r^2 = 0.90$) and Toplis and Carroll (1995) ($n = 21$; $r^2 = 0.90$)

wards when plagioclase and ilmenite are the two liquidus phases and MgO thus behaves as an incompatible element. When orthopyroxene and olivine appear as liquidus phases, both MgO in ilmenite and the Mg# of orthopyroxene start decreasing with differentiation. MgO becomes compatible. MgO in ilmenite from the Skaergaard intrusion also linearly decreases with differentiation (Jang and Naslund 2003), because the Mg# of the magma progressively decreases due to fractionation of mafic minerals.

This simple interpretation is complicated by two facts. First, the parental magma of the Tellnes deposit

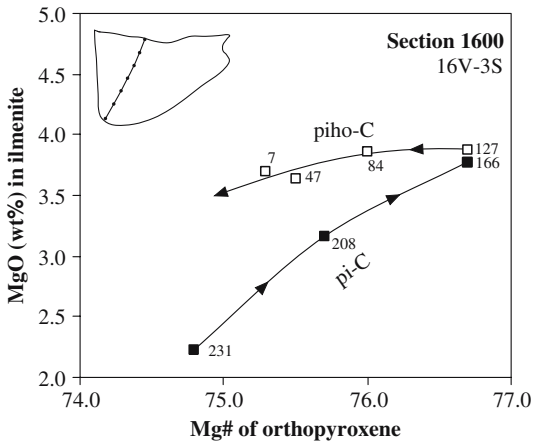

Fig. 9 MgO (wt%) in ilmenite as a function of Mg# (= Mg/Mg + Fe) of orthopyroxene in section 1600 of the Tellnes deposit. Numbers are depths (in meters) for each sample. *Filled squares* are plagioclase-ilmenite cumulates (*pi-C*), *open squares* are plagioclase-ilmenite-orthopyroxene-olivine cumulates (*piho-C*)

contains 5.2% MgO (sample 12.5 V-6 S, 264; Charlier et al. 2006), a value in the range for primitive jotunites of the Rogaland Anorthosite Province (4.6–6% MgO). This implies that, for $D^{\mathrm{Ilm}}_{\mathrm{MgO}} = 1.35$ from experiments, the first ilmenite to crystallize should contain ca. 7% MgO. This is significantly higher than the MgO content of the most primitive ilmenite in the ore body, based on its Cr content (sample 12.5 V-6 S, 239; MgO = 3.49%). Secondly, Fig. 10a, which displays MgO versus Cr in ilmenite, has two different trends in sections 1200 and 1600 and the compositions of the most primitive ilmenite in each section does not lie on the same fractionation path. This would imply different values for $D^{\mathrm{Ilm}}_{\mathrm{MgO}}$ and $D^{\mathrm{Ilm}}_{\mathrm{Cr}}$ and/or different parental magmas for each section.

The theoretical trend for the evolution of MgO in ilmenite has been calculated by the following method. The parental magma contains 5.2 wt% MgO (Charlier et al. 2006) and the first cumulus ilmenite should contain 7.0 wt% MgO (with $D^{\mathrm{Ilm}}_{\mathrm{MgO}} = 1.35$). Because the cotectic proportion of ilmenite is 17.5% and Mg is only present in ilmenite, the fractionating pi-cumulates contain $7\% \times 0.163 = 1.225$ wt% MgO. The bulk partition coefficient of MgO between pi-cumulates and melt is thus $D^{\mathrm{Bulk}}_{\mathrm{MgO}} = 1.225/5.2 = 0.24$. From the application of the Rayleigh equation, it emerges that for $F = 0.8$, just before the appearance of cumulus orthopyroxene and olivine, the MgO content of the liquid is 6.16 wt% and MgO in ilmenite is 8.32 wt%. This trend is reproduced in Fig. 10a.

The difference between the theoretical cumulus MgO content of ilmenite and the observed content (Fig. 10a) reflects extensive postcumulus re-equilibration. The distribution of Fe^{2+} and Mg between coexisting ilmenite and orthopyroxene, calibrated experimentally as a function of temperature, pressure, and composition of the coexisting phases by Bishop (1980), is able to account for the discrepancies between theoretical and observed MgO contents in ilmenite. The equation is

$$T\,(^{\circ}\mathrm{C}) = ((1646 + 1634[\mathrm{Fe}^{2+}/(\mathrm{Fe}^{2+} + \mathrm{Mg})]^{\mathrm{Ilm}} + 0.0124P)/\ln K_D) - 273$$

with $K_D = (\mathrm{Mg/Fe})^{\mathrm{Opx}}/(\mathrm{Mg/Fe})^{\mathrm{Ilm}}$, and P in bars, estimated at 5,000 bars (Charlier et al. 2006). Fig. 10b displays two profiles of temperature calculated with the equation of Bishop (1980) versus stratigraphy in sections 1200 and 1600. Both profiles have increasing temperatures from the bottom to the upper part of the intrusion around 820–850°C. Lower MgO contents in ilmenite from the lower part of the intrusion result from equilibration with orthopyroxene at a lower

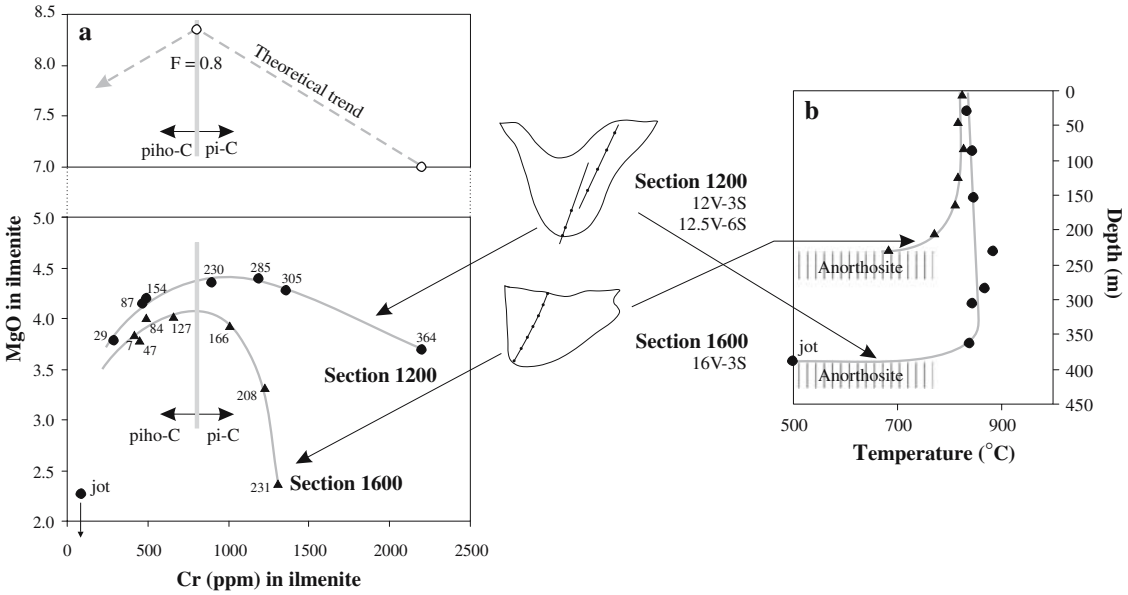

Fig. 10 **a** MgO versus Cr in cumulus ilmenite (with their depth) corrected for the trapped liquid shift in selected drill-cores in sections 1200 and 1600 of the Tellnes deposit and theoretical trend for the evolution of the MgO content in cumulus ilmenite. **b** Depth versus equilibrium temperature for the distribution of Mg and Fe^{2+} between ilmenite and orthopyroxene calculated from Bishop (1980). *Jot* is the ilmenite composition in the chilled jotunitic parental magma located at the contact with the host anorthosite

temperature. Because the most primitive ilmenite compositions is at the base of section 1200, the first crystallizing liquidus phases have unquestionably accumulated in this part of the intrusion. In other parts of the deposit (e.g. in section 1600), more evolved cumulates have crystallized under identical thermal conditions because they are located at the same distance from the host anorthosite compared to more primitives cumulates at the base of section 1200. This explains the two different evolution trends in Fig. 10a, which actually represent two different postcumulus evolutions.

The reason for this higher degree of re-equilibration of Mg in ilmenite at the margins of the ore body is not obvious. A higher rate of cooling is expected at the margins, which would tend to preclude extensive re-equilibration that is favoured by slow cooling. However, marginal zones are characterized by a continuously increasing proportion of trapped liquid towards the contact with the anorthosite (Charlier et al. 2006). Consequently, the presence of large amount of interstitial liquid has facilitated postcumulus exchanges of MgO between cumulus ilmenite and melt. This postcumulus solid–liquid exchange, which was more efficient with high TLF, was prolonged by subsolidus interactions with ferromagnesian silicates and between oxides.

Similar interpretation might be reached for ilmenite composition in the Skaergaard intrusion where the MgO content in ilmenite is higher in the Layered Series compared to the Upper Border Series, where it is higher than in the Marginal Border Series for similar fraction of crystallization (Jang and Naslund 2003). This probably results from increasing TLF in these different series.

Exsolved pleonaste: a sink for the missing Mg of ilmenite?

The exsolution of pleonaste from ilmenite (Fig. 4a) could have a significant effect on the MgO content of ilmenite. Indeed, when external granules are produced, these are not included in the bulk analysis of ilmenite. Small rounded grains of pleonaste close to ilmenite, and not included in it, probably result from this mechanism. The amount of MgO exsolved from ilmenite as pleonaste can be quantitatively evaluated through the difference between the Al_2O_3 content of ilmenite predicted by experimental partition coefficients and the actual Al_2O_3 content of analysed ilmenite. The average Al_2O_3 content in ilmenite determined by LA-ICP-MS is ca. 0.08 wt% (eTable 2). Partition coefficients for Al_2O_3 between ilmenite and the melt calculated from the experiments of Snyder et al. (1993), Vander Auwera and Longhi (1994) and Toplis and Carroll (1995) are 0.026, 0.033 and 0.029, respectively. Consequently, considering Al_2O_3 = 16.1% for the Tellnes parental magma (Charlier et al. 2006),

the Al_2O_3 content of liquidus ilmenite should be between 0.42 and 0.53%. The difference between primary and re-equilibrated ilmenite is between 0.34 and 0.45% which is probably expelled as pleonaste exsolutions. Because pleonaste contains 61.2% Al_2O_3 and 16.9% MgO on average (K. Kullerud, unpublished data), the amount of MgO expelled from ilmenite as pleonaste exsolutions is 0.09–0.14%, which has no influence on the MgO content of ilmenite.

Zr in ilmenite, zircon coronas and timing of emplacement of the Tellnes deposit

XRF data on separated ilmenite display a range from 58 to 554 ppm (eTable 1). These values are considerably higher than data obtained by in situ LA-ICP-MS (eTable 2), where Zr varies between 8 and 114 ppm (Fig. 11). According to XRF data, Zr in ilmenite increases with decreasing Cr in ilmenite, because of the incompatible behaviour of Zr. However, LA-ICP-MS Zr data remain constant for a wide range of Cr values. Consequently, as illustrated by samples analysed by both methods, large discrepancies are observed in the two analytical methods. These variations do not result from the calibration of the analytical methods because of the unsystematic character of the shift. Hf from LA-ICP-MS (eTable 2) is correlated with Zr and thus behaves similarly.

The observed decoupling between XRF analyses of bulk ilmenite concentrate and in situ LA-ICP-MS analyses of ilmenite is explained by the microtextures illustrated in Figs. 4a–c. Ilmenite commonly contains baddeleyite inclusions and is rimmed by a zircon corona. Such microtextures are known from the literature. Naslund (1987) has described baddeleyite lamellae in ilmenite from the tholeiitic Basistoppen sill. Zircon, baddeleyite and srilankite (Ti_2ZrO_6) associated with ilmenite have also been described by Bingen et al. (2001) in high-grade metaanorthosite-norite rocks of Western Norway. These microtextures are interpreted as the result of decreasing solubility of Zr in ilmenite with decreasing temperature and consequent exsolution of ZrO_2. Baddeleyite represents exsolution granules and zircon is regarded as a product of a reaction between baddeleyite and available silica during metamorphism. The Zr concentration data in the Tellnes deposit (eTable 4) shows that 82% in average is not residing in the ilmenite lattice itself but is sequestrated in baddeleyite and zircon attached to ilmenite. The comparatively low and uniform in situ Zr concentration in ilmenite and the lack of correlation between in situ Zr concentration and Cr concentration or stratigraphic position of the sample in the deposit strongly support the exsolution interpretation and rules out an interpretation involving epitaxial growth of baddeleyite and ilmenite or zircon and ilmenite during the cumulus or postcumulus phases. As opposed to the occurrences of zircon coronas in Western Norway (Bingen et al. 2001), the Tellnes deposit is not showing any evidence for metamorphic overprint, so the formation of zircon coronas can be integrated in the postcumulus evolution or subsolidus cooling of the magma chamber, and not attributed to a subsequent metamorphic event. Whether or not the zircon coronas formed in the presence of residual interstitial melt is difficult to assess from the data. Mass balance calculation using Zr concentration in whole rock, Zr in ilmenite from XRF and LA-ICP-MS, and the proportion of ilmenite (eTable 4) shows that, in average, 8% of Zr is hosted in ilmenite lattice, 20% is in zircon and baddeleyite attached to ilmenite and 72% is in zircon and baddeleyite not attached to ilmenite, either formed by crystallization of trapped liquid or from coalescence of exsolved granules.

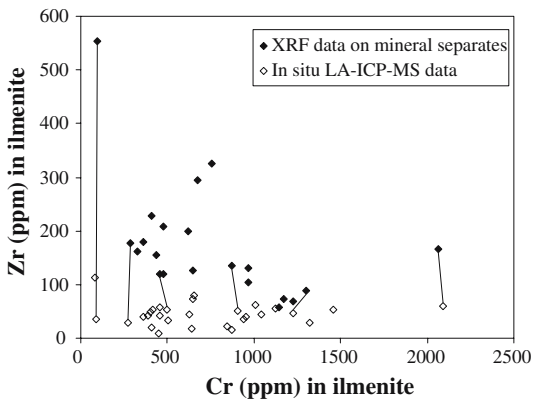

Fig. 11 Zr versus Cr in ilmenite from the Tellnes deposit from XRF and LA-ICP-MS analyses. *Lines* join samples analysed by both methods

A typical sample of ilmenite norite from the Tellnes deposit provided a zircon U-Pb age of 920 ± 3 Ma and an equivalent baddeleyite age of 923 ± 7 Ma (Schärer et al. 1996). The age of 920 ± 3 Ma is derived from two concordant multigrain zircon fractions described as "large grains and fragments", presumably anhedral, and the age of 923 ± 7 Ma from three near-concordant multigrain baddeleyite fractions. No isolated zircon grain with evident prismatic magmatic habit has been observed by petrographic examinations, in line with the interpretation that zircon is not a cumulus phase. All observed zircon grains are systematically closely associated with ilmenite. The large zircon grains analysed by Schärer et al. (1996) possibly formed from crystallization of interstitial trapped melt or, more

probably, as suggested by the thick corona texture illustrated in Fig. 4c, from coalescence of micro-zircons or zircon coronas formed after exsolution from ilmenite. Consequently, the zircon age of 920 ± 3 Ma possibly records crystallization of the interstitial melt or more probably exsolution of Zr from ilmenite. It certainly does not record crystallization of the cumulate. The occurrence of a chilled margin indicates that the Tellnes deposit is younger than the host Åna-Sira anorthosite pluton. The intrusion age of the Åna-Sira pluton is estimated at 932 ± 3 Ma, as provided by oscillatory zoned zircon associated with high-alumina orthopyroxene megacrysts in the anorthosite, and 931 ± 5 Ma, as provided by zircon from a quartz mangerite dyke. It can be concluded that intrusion of the Tellnes deposit took place between 932 ± 3 and 920 ± 3 Ma, and that the Tellnes deposit is marginally younger than the large anorthosite plutons hosting it.

Emplacement mechanism of the Tellnes ilmenite deposit

The cotectic proportion of ilmenite (17.5 wt%) is much lower than its modal proportion in the Tellnes deposit (up to 50 wt%; Charlier et al. 2006). Dynamic sorting during flow of a crystal mush, as proposed by Wilmart et al. (1989), would be an efficient way of producing a higher rate of ilmenite accumulation compared to other less-dense liquidus phases. However, this emplacement mechanism can hardly produce: (1) the continuous stratigraphically decreasing contents of compatible elements and increasing contents of incompatible elements in ilmenite; (2) the succession of two cumulus assemblages (Fig. 2); (3) the systematic evolution of the magnetite content (Fig. 3). These vertical trends are also laterally consistent throughout the ore body.

In accordance with the interpretation of Charlier et al. (2006), we propose that the Tellnes cumulates crystallized in situ. The high proportion of ilmenite results from the high density contrast between ilmenite (ca. 4.7 g cm^3) and plagioclase (An_{50}: 2.6 g cm^3) and from the high density of the iron-rich jotunitic parental magma (ca. 2.75 g cm^3, Scoates 2000; Vander Auwera et al. 2006) in which plagioclase was probably buoyant. We have concluded that the fraction of magma remaining after the crystallization of the exposed portion of the Tellnes deposit is ca. 60%. The bulk fractionated cumulate thus represents 40% crystallization of the parental magma (Fig. 12). This bulk cumulate includes rocks exposed in the deposit and the fraction of floating plagioclase. These floating plagioclases are indeed the complementary liquidus phases to the non-cotectic cumulates of the ore body. Consequently, the unexposed upper part of Tellnes, which includes the residual liquid and the missing mass of plagioclase removed by flotation, represents some 86% of the initial magma.

Flotation of plagioclase is a common explanation of the formation of massif-type anorthosites (Ashwal 1993). This model is extended here to the formation of an ilmenite-rich norite in a small magma chamber intruded in a large anorthosite pluton.

Conclusions

Ilmenite compositional variation with stratigraphic height indicates that fractional crystallization was the major process responsible for differentiation in the Tellnes ilmenite deposit. Modelling by the Rayleigh equation constrains the fraction of residual liquid to be ca. 0.8 after crystallization of the first cumulus assemblage (pi-C) and to ca. 0.6 after piho-C from volume estimation. Calculations of the cotectic proportions of ilmenite in pi-C give a value of 17.5%, significantly lower than the proportion of cumulus ilmenite in the deposit (ca. 50%). This implies sorting of ilmenite and its preferential accumulation at the bottom of the chamber. Accumulation of ilmenite first took place in

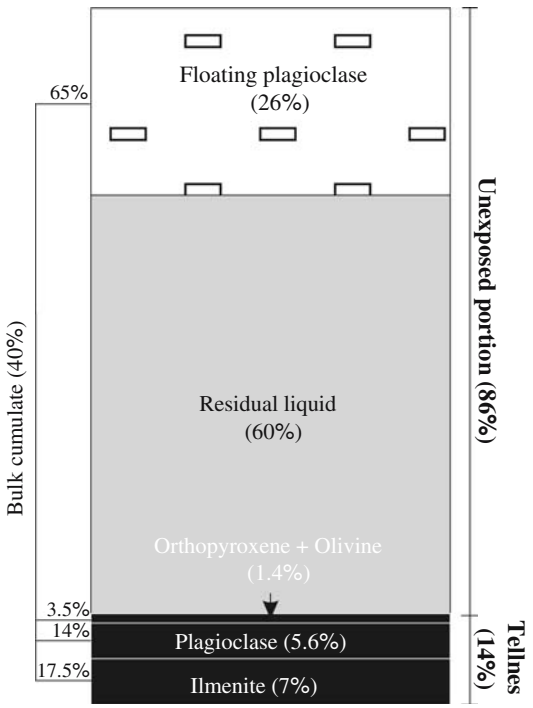

Fig. 12 Synthetic model for the Tellnes ilmenite deposit with the relative proportion (wt%) of the different constituents calculated by the fractional crystallization model

the vicinity of section 1200 of the ore body, where the base of the chamber was probably originally deeper. The exposed portion of the Tellnes deposit represents the lower part (14%) of a larger magma chamber. The unexposed upper part contained the missing mass of plagioclase removed by flotation and the crystallization products of the residual liquid.

The crystallization of ilmenite from trapped liquid and subsolidus re-equilibration have affected the primary composition of liquidus ilmenite. The MgO content of ilmenite has been significantly lowered by extensive solid–liquid exchange prolonged by re-equilibration with Fe-Mg silicates, especially at the margins of the ore body where the trapped liquid proportion was higher. Different thermal conditions in different parts of the intrusion for the same degree of differentiation of the magma have resulted in variable subsolidus evolution paths for MgO in ilmenite.

Finally, exsolution of zircon from ilmenite put into question the interpretation of the age of 920 ± 3 Ma obtained by Schärer et al. (1996). This delay of 10 Ma compared with the anorthosite crystallization ages corresponds to the timing of exsolution and not to the crystallization age of the Tellnes deposit.

Acknowledgments This work was funded by the Belgian Fund for Joint Research and the Fund for Research in Industry and Agriculture (FRIA). TITANIA A/S and the Geological Survey of Norway are gratefully acknowledged for their financial support and permission to use unpublished data. Guy Bologne is thanked for assistance with XRF analyses. We also acknowledge Kåre Kullerud for sharing unpublished microprobe data. This paper has benefited from constructive comments by Brian Robins, Richard Wilson and Gurli Meyer. Reviews by Mike Toplis, Bernard Bingen and Grant Cawthorn helped us improve the manuscript.

References

Andersen DJ, Lindsley DH, Davidson PM (1993) QUILF: a PASCAL program to assess equilibria among Fe-Mg-Ti oxides, pyroxenes, olivine, and quartz. Comput Geosci 19:1333–1350

Ashwal LD (1993) Anorthosites. Springer, Heidelberg, p 422

Barnichon J-D, Havenith H, Hoffer B, Charlier R, Jongmans D, Duchesne JC (1999) The deformation of the Egersund Ogna massif, South Norway: finite element modelling of diapirism. Tectonophysics 303:109–130

Bingen B, van Breemen O (1998) U-Pb monazite ages in amphibolite- to granulite-facies orthogneiss reflect hydrous mineral breakdown reactions: Sveconorwegian province of SW Norway. Contrib Mineral Petrol 132:336–353

Bingen B, Stein HJ (2003) Molybdenite Re-Os dating of biotite dehydration melting in the Rogaland high-temperature granulites, S. Norway. Earth Planet Sci Lett 208:181–195

Bingen B, Demaiffe D, van Breemen O (1998) The 616-My-old Egersund basaltic dike swarm, SW Norway, and the late Proterozoic opening of the Iapetus Ocean. J Geol 106:565–574

Bingen B, Austrheim H, Whitehouse M (2001) Ilmenite as a source for zirconium during high-grade metamorphism? Textural evidence from the Caledonides of Western Norway and implications for zircon geochronology. J Petrol 42:355–375

Bingen B, Stein HJ, Bogaerts M, Bolle O, Mansfeld J (2006) Molybdenite Re-Os dating constrains gravitational collapse of the Sveconorwegian orogen, SW Scandinavia. Lithos 87:328–346

Bishop FC (1980) The distribution of Fe^{2+} and Mg between coexisting ilmenite and pyroxene with applications to geothermometry. Am J Sci 280:46–77

Bolle O (1996) Mélanges magmatiques et tectonique gravitaire dans l'Apophyse de l'intrusion de Bjerkreim-Sokndal (Rogaland, Norvège). Pétrologie, géochimie et fabrique magnétique. Ph.D. Thesis, Université de Liège, p 204

Bolle O, Trindade RIF, Bouchez JL, Duchesne JC (2002) Imaging downward granitic magma transport in the Rogaland Igneous Complex, SW Norway. Terra Nova 14:87–92

Cawthorn RG, Biggar GM (1993) Crystallization of titaniferous chromite, magnesian ilmenite and armacolite in tholeiitic suites in the Karoo Igneous Province. Contrib Mineral Petrol 114:221–235

Charlier B, Duchesne J-C, Vander Auwera J (2006) Magma chamber processes in the Tellnes ilmenite deposit (Rogaland Anorthosite Province, SW Norway) and the formation of Fe-Ti ores in massif-type anorthosites. Chem Geol 234:264–290

Duchesne JC (1972) Iron-titanium oxide minerals in the Bjerkrem-Sogndal Massif, South-western Norway. J Petrol 13:57–81

Duchesne JC (1999) Fe-Ti deposits in Rogaland anorthosites (South Norway): geochemical characteristics and problems of interpretation. Mineralium Deposita 34:182–198

Duchesne JC, Maquil R, Demaiffe D (1985) The Rogaland anorthosites: facts and speculations. In: Tobi AC, Touret JLR (eds) The deep proterozoic crust in the North Atlantic province. NATO Adv Stud Inst, Dordrecht, pp 449–476

Duchesne JC, Liégeois JP, Vander Auwera J, Longhi J (1999) The crustal tongue melting model and the origin of massive anorthosites. Terra Nova 11:100–105

Frost BR, Lindsley DH, Andersen DJ (1988) Fe-Ti oxide-silicate equilibria: assemblages with fayalitic olivine. Am Mineral 73:727–740

Irvine TN (1982) Terminology for layered intrusions. J Petrol 23:127–162

Jang YD, Naslund HR (2003) Major and trace element variation in ilmenite in the Skaergaard intrusion: petrologic implications. Chem Geol 193:109–125

Jensen JC, Nielsen FM, Duchesne JC, Demaiffe D, Wilson JR (1993) Magma influx and mixing in the Bjerkreim-Sokndal layered intrusion, South Norway: evidence from the boundary between two megacyclic units at Storeknuten. Lithos 29:311–325

Kennedy AK, Lofgren GE, Wasserburg GJ (1993) An experimental study of trace element partitioning between olivine, orthopyroxene and melt in chondrules: equilibrium values and kinetic effects. Earth Planet Sci Lett 115:177–195

Krause H, Gierth E, Schott W (1985) Ti-Fe deposits in the South Rogaland igneous complex, especially in the anorthosite-massif of Åna-Sira. Norges Geologiske Undersøkelese 402:25–37

Naslund HR (1987) Lamellae of baddeleyite and Fe-Cr-spinel in ilmenite from the Basistoppen sill, East Greenland. Can Mineral 25:91–96

Ødegaard M, Skår Ø, Schiellerup H, Pearson NJ (2005) Preparation of a synthetic titanite glass calibration material for in situ microanalysis by direct fusion in graphite electrodes: a preliminary characterisation by EPMA and LA-ICP-MS. Geostand Geoanal Res 29:197–209

Rayleigh JWS (1896) Theoretical considerations respecting the separation of gases. Philos Mag 42:493–498

Schärer U, Wilmart E, Duchesne JC (1996) The short duration and anorogenic character of anorthosite magmatism: U-Pb dating of the Rogaland complex, Norway. Earth Planet Sci Lett 139:335–350

Scoates JS (2000) The plagioclase-magma density paradox re-examined and the crystallization of Proterozoic anorthosites. J Petrol 41:627–649

Snyder D, Carmichael ISE, Wiebe RA (1993) Experimental study of liquid evolution in an Fe-rich, layered mafic intrusion: constrains of Fe-Ti oxide precipitation on the T-fO_2 and T-ρ paths of tholeiitic magmas. Contrib Mineral Petrol 113:73–86

Toplis MJ, Carroll MR (1995) An experimental study of the influence of oxygen fugacity on Fe-Ti oxide stability, phase relations, and mineral-melt equilibria in ferro-basaltic systems. J Petrol 36:1137–1170

Toplis MJ, Corgne A (2002) An experimental study of element partitioning between magnetite, clinopyroxene and iron-bearing silicate liquids with particular emphasis on vanadium. Contrib Mineral Petrol 144:22–37

Toplis MJ, Libourel G, Carroll MR (1994) The role of phosphorous in crystallization processes of basalt: An experimental study. Geochimica et Cosmochimica Acta 58:797–810

van Achterbergh E, Ryan CG, Jackson SE, Griffin WL (2001) Data reduction software for LA-ICP-MS. In: Sylvester P (ed) Laser-ablation-ICPMS in the earth sciences: principles and applications. Mineralogical Association of Canada, Short Course 29, pp 239–243

Vander Auwera J, Longhi J (1994) Experimental study of a jotunite (hypersthene monzodiorite): constraints on the parent magma composition and crystallization conditions (P, T, f_{O2}) of the Bjerkreim-Sokndal layered intrusion (Norway). Contrib Mineral Petrol 118:60–78

Vander Auwera J, Longhi J, Duchesne JC (2000) The effect of pressure on D_{Sr} (plag/melt) and D_{Cr} (opx/melt): implications for anorthosite petrogenesis. Earth Planet Sci Lett 178:303–314

Vander Auwera J, Longhi J, Duchesne JC (2003) Some results on the role of P, T and fO_2 on ilmenite composition. Norges geologiske undersøkelse Spec Publ 9:35–37

Vander Auwera J, Weis D, Duchesne JC (2006) Marginal mafic intrusions as indicators of downslope draining of dense residual melts in anorthositic diapirs? Lithos 89:329–352

Wilmart E, Demaiffe D, Duchesne JC (1989) Geochemical constraints on the genesis of the Tellnes ilmenite deposit, Southwest Norway. Econ Geol 84:1047–1056

Wilson JR, Robins B, Nielsen FM, Duchesne JC, Vander Auwera J (1996) The Bjerkreim-Sokndal layered intrusion, Southwest Norway. In: Cawthorn RG (ed) Layered intrusions. Elsevier, Amsterdam, pp 231–255